Acta Crystallographica Section A
Foundations of Crystallography
ISSN 0108-7673

Received 19 January 2011
Accepted 9 February 2011

Variance of electron-density maps in space group *P*1

Carmelo Giacovazzo[a,b]* and Annamaria Mazzone[a]

[a]Institute of Crystallography CNR, Via G. Amendola, 122/O, 70126 Bari, Italy, and [b]Dipartimento Geomineralogico, University of Bari, Campus Universitario, Bari, Italy. Correspondence e-mail: carmelo.giacovazzo@ic.cnr.it

The expected mean-square error of electron-density maps (observed and difference) is traditionally estimated as a function of the variance of the observed amplitudes. The usual purpose is to evaluate the reliability of the structural parameters suggested by the final electron-density maps. Accordingly, such calculations are performed after the refinement stage, when the phases are considered perfectly determined. In this paper a mathematical expression for the variance (observed, difference and hybrid) is obtained for each point of an electron-density map for the space group $P1$ under a different hypothesis: the current phases are distributed on the trigonometric circle about the correct values, according to von Mises distributions. The variance calculation may then be performed at any stage of the phasing process, starting from a random up to a highly correlated model. It has been shown that the variance does not change dramatically from point to point of the map; therefore emphasis has been given to the concept of *map variance*, which allows an easier study of its properties. When the model is highly correlated with the target structure the conclusive formulas reduce to those previously described in the literature. The properties of the variance are discussed: it is shown that they are the basis for the most successful phasing procedures.

1. Notation

NREF: number of observed reflections (Friedel opposite included).
$F = \sum_{j=1}^{N} f_j \exp(2\pi i \mathbf{h}\mathbf{r}_j) = |F| \exp(i\varphi)$: structure factor of the target structure.
$F_p = \sum_{j=1}^{p} f_j \exp(2\pi i \mathbf{h}\mathbf{r}'_j) = |F_p| \exp(i\varphi_p)$, where $\mathbf{r}'_j = \mathbf{r}_j + \Delta\mathbf{r}_j$: structure factor of the model structure.
$\sum_N = \sum_{j=1}^{N} f_j^2$.
$\sum_p = \sum_{j=1}^{p} f_j^2$.
$F_q = F - F_p = |F_q| \exp(i\varphi_q)$: structure factor of the *ideal difference structure*.
$E = A + iB = R\exp(i\varphi)$, $E_p = A_p + iB_p = R_p \exp(i\varphi_p)$, $E_q = A_q + iB_q = R_q \exp(i\varphi_q)$, $R = |F|/\sum_N^{1/2}$, $R_p = |F_p|/\sum_N^{1/2}$.
$\rho(\mathbf{r}) = (2/V)\sum_{\mathbf{h}>0} |F_\mathbf{h}| \cos(2\pi\mathbf{h}\cdot\mathbf{r} - \varphi_\mathbf{h})$: general expression of an electron-density map.
$\rho_p(\mathbf{r}) = (2/V)\sum_{\mathbf{h}>0} |F_{p\mathbf{h}}| \cos(2\pi\mathbf{h}\cdot\mathbf{r} - \varphi_{p\mathbf{h}})$: electron-density map of the model structure.
$\rho_{\rm obs}(\mathbf{r}) = (2/V)\sum_{\mathbf{h}>0} m_\mathbf{h} |F_\mathbf{h}| \cos(2\pi\mathbf{h}\cdot\mathbf{r} - \varphi_{p\mathbf{h}})$: observed electron density when a model is available.
$[\rho(\mathbf{r})]_N = (2/V)\sum_{\mathbf{h}>0} R_\mathbf{h} \cos(2\pi\mathbf{h}\cdot\mathbf{r} - \varphi_\mathbf{h})$: electron-density map calculated *via* normalized structure factors.
$\rho_{pN}(\mathbf{r}) = (2/V)\sum_{\mathbf{h}>0} R_{p\mathbf{h}} \cos(2\pi\mathbf{h}\cdot\mathbf{r} - \varphi_{p\mathbf{h}})$: electron-density map of the model structure calculated *via* normalized structure factors.
$\rho_{{\rm obs}N}(\mathbf{r}) = (2/V)\sum_{\mathbf{h}>0} m_\mathbf{h} R_\mathbf{h} \cos(2\pi\mathbf{h}\cdot\mathbf{r} - \varphi_{p\mathbf{h}})$: observed electron density when a model is available calculated *via* normalized structure factors.
$P(\mathbf{u}) = (2/V)\sum_{\mathbf{h}>0} |F_\mathbf{h}|^2 \cos(2\pi\mathbf{h}\mathbf{u})$: Patterson synthesis.

In all the above Fourier syntheses (observed, difference, hybrid) the term of order zero is omitted. Accordingly, the average values of the corresponding maps are always zero. By $\mathbf{h} > 0$ it is meant that the summation is over one half of the reciprocal space (only one member of each Friedel pair is included).

$\mathrm{var}_\rho(\mathbf{r}) = \langle[\rho(\mathbf{r})]^2\rangle - [\langle\rho(\mathbf{r})\rangle^2]$: variance of the map ρ in a point $\mathbf{r}$.
$[\mathrm{var}_\rho(\mathbf{r})]_N = \langle[\rho(\mathbf{r})]_N{}^2\rangle - \{\langle[\rho(\mathbf{r})]_N\rangle^2\}$: variance of the normalized electron-density map.
$D_i(x) = I_i(x)/I_0(x)$: I_i is the modified Bessel function of order i.
EDM: electron-density modification.
$D = \langle\cos(2\pi\mathbf{h}\Delta\mathbf{r})\rangle$: the average is performed per resolution shell.
$\sigma_A = D(\Sigma_p/\Sigma_N)^{1/2}$.
$\sigma_R^2 = \langle|\mu|^2\rangle/\sum_N$: $\langle|\mu|^2\rangle$ is the measurement error.
$e = 1 + \sigma_R^2$.
$m = \langle\cos(\varphi - \varphi_p)\rangle = I_1(X)/I_0(X)$ where $X = 2\sigma_A R R_p \times (e - \sigma_A^2)^{-1}$.

$s = \sin\theta/\lambda$.
CORR: correlation between the model and the target electron-density maps.

2. Introduction

In the early days of modern crystallography much effort was dedicated to establishing the accuracy of the results of structure analysis. In this context the study of electron density played a major role (Bragg & West, 1930; Booth, 1946, 1947; Cruickshank, 1949; Cochran, 1951; Cruickshank & Rollett, 1953) with special attention paid to the effect of measurement errors. In particular, the expected mean-square error in the electron-density map was estimated (Cruickshank, 1949) as

$$\sigma^2(\rho) = \frac{1}{V^2}\sum_{\mathbf{h}} \sigma^2(|F_{\mathbf{h}}|), \tag{1}$$

where $\sigma^2(|F_{\mathbf{h}}|)$ is the variance of the observed amplitude. Equation (1) provides a global error, constant for any point of the map. More interesting results were obtained by Coppens & Hamilton (1968), who obtained error functions at specific points in the unit cell:

$$\sigma^2[\rho(\mathbf{r})] = \frac{4}{V^2}\sum_{\mathbf{h}>0} \sigma^2(|F_{\mathbf{h}}|)\cos^2(2\pi\mathbf{h}\cdot\mathbf{r} - \varphi_{\mathbf{h}}). \tag{2}$$

All the above works addressed interpretation of the maps obtained in the final stages of crystal structure refinement (when the phases are considered perfectly determined and therefore fixed), to assess the reliability of the conclusive structural parameters. In this paper we will calculate the expected value of the electron-density map ρ and its variance $\mathrm{var}_\rho(\mathbf{r})$ in any point $\mathbf{r}$ of the map when:

(*a*) No information on the phases is available (in practice no model structure is available). Then the phases $\varphi_{\mathbf{h}}$ may be considered random variables uniformly distributed on the trigonometric circle.

(*b*) A model structure is available. Then each phase $\varphi_{\mathbf{h}}$ may be considered to be distributed around $\varphi_{p\mathbf{h}}$ according to the von Mises distribution $M(\varphi; X, \varphi_p)$ where

$$M(\varphi; X, \varphi_p) = [2\pi I_0(X)]^{-1}\exp[X\cos(\varphi - \varphi_p)]. \tag{3}$$

Equation (3) is the most used and most accurate phase distribution when a model structure is available. It originates from the study (Srinivasan & Ramachandran, 1965) of the joint probability distribution $P(E_{\mathbf{h}}, E_{p\mathbf{h}})$ of which equation (3) is a conditional distribution. It may be applied in quite a wide range of examples, from the case in which the model is uncorrelated with the structure [*i.e.* equivalent to case (*a*) above], to the limit case in which the model coincides with the structure {then the distribution [equation (3)] becomes a Dirac delta function centred on φ_p}. It may be concluded that the distribution [equation (3)] is particularly useful for the purposes of this paper, aiming at estimating the variance of an electron-density map no matter the quality of the model structure.

We are also interested in the variance of the difference Fourier syntheses and in general in that of the hybrid syntheses of type $\tau F - \omega F_p$. We use our mathematical results to provide a key for interpreting various phasing algorithms, among which we quote EDM techniques, charge flipping and the VLD algorithm.

3. The estimate of $\mathrm{var}_\rho(\mathbf{r})$ in *P*1

We analyse the cases (*a*) and (*b*) of §2.

Case (*a*): phases φ are randomly distributed on the trigonometric circle. Since $\langle\cos(2\pi\mathbf{h}\cdot\mathbf{r} - \varphi_{\mathbf{h}})\rangle = 0$ for any $\mathbf{r}$,

$$\langle\rho(\mathbf{r})\rangle = 0 \tag{4}$$

for any point $\mathbf{r}$ of the map. This is a reasonable result; in the absence of a model correlated with the electron density of the target structure, $\rho(\mathbf{r})$ may have positive or negative values with the same probability in any point of the map. Since

$$\langle[\rho(\mathbf{r})]^2\rangle = \frac{4}{V^2}\sum_{\mathbf{h},\mathbf{k}>0}\langle|F_{\mathbf{h}}F_{\mathbf{k}}|\cos(2\pi\mathbf{h}\mathbf{r} - \varphi_{\mathbf{h}})\cos(2\pi\mathbf{k}\mathbf{r} - \varphi_{\mathbf{k}})\rangle,$$

the only non-vanishing contributions to the average occur when $\mathbf{h} = \mathbf{k}$ (we deliberately neglect the cases for which $\mathbf{k} = n\mathbf{h}$, where n is an integer number: their contribution is non-vanishing only for very small n values). Therefore

$$\langle[\rho(\mathbf{r})]^2\rangle = \frac{2}{V^2}\sum_{\mathbf{h}>0}|F_{\mathbf{h}}|^2 = \frac{1}{V}P(\mathbf{0}),$$

which is constant for any point of the map. Accordingly

$$\mathrm{var}_\rho(\mathbf{r}) = \frac{1}{V}P(\mathbf{0}). \tag{5}$$

If normalized structure factors are used as coefficients of the Fourier synthesis, then

$$\langle[\rho(\mathbf{r})]_N\rangle = 0 \quad \text{and} \quad [\mathrm{var}_\rho(\mathbf{r})]_N = \mathrm{NREF}/V. \tag{6}$$

In conclusion, when no information is available on the phases, the variance $\mathrm{var}_\rho(\mathbf{r})$ and $[\mathrm{var}_\rho(\mathbf{r})]_N$ do not vary with $\mathbf{r}$. Increasing the data resolution leads to higher values of the variance; in particular $[\mathrm{var}_\rho(\mathbf{r})]_N$ is equal to the measured reciprocal-space volume.

Case (*b*): phases are distributed according to equation (3). This case implies that a model (no matter if poor or accurate) is available. Then

$$\langle\rho(\mathbf{r})\rangle = \frac{2}{V}\sum_{\mathbf{h}>0} m_{\mathbf{h}}|F_{\mathbf{h}}|\cos(2\pi\mathbf{h}\cdot\mathbf{r} - \varphi_{p\mathbf{h}}) = \rho_{\mathrm{obs}}(\mathbf{r}). \tag{7}$$

If the model is uncorrelated with the target structure then $\sigma_A = 0$ for any $\mathbf{h}$ and $\langle\rho(\mathbf{r})\rangle = 0$, as in case (*a*). If $\sigma_A = 1$ the distribution of each φ is a delta function centred on φ_p and $\langle\rho(\mathbf{r})\rangle \equiv \rho_p(\mathbf{r})$.

In general

$$\begin{aligned}\langle\rho^2(\mathbf{r})\rangle &= \frac{4}{V^2}\sum_{\mathbf{h},\mathbf{k}>0}\langle|F_\mathbf{h}F_\mathbf{k}|\cos(2\pi\mathbf{h}\cdot\mathbf{r}-\varphi_\mathbf{h})\cos(2\pi\mathbf{k}\mathbf{r}-\varphi_\mathbf{k})\rangle\\ &= \frac{4}{V^2}\sum_{\mathbf{h}>0}|F_\mathbf{h}|^2\langle\cos^2(2\pi\mathbf{h}\cdot\mathbf{r}-\varphi_\mathbf{h})\rangle\\ &\quad+\frac{4}{V^2}\sum_{\mathbf{h}\neq\mathbf{k}>0}|F_\mathbf{h}F_\mathbf{k}|\langle\cos(2\pi\mathbf{h}\cdot\mathbf{r}-\varphi_\mathbf{h})\cos(2\pi\mathbf{k}\mathbf{r}-\varphi_\mathbf{k})\rangle\\ &= \frac{2}{V^2}\sum_{\mathbf{h}>0}|F_\mathbf{h}|^2+\frac{2}{V^2}\sum_{\mathbf{h}>0}|F_\mathbf{h}|^2D_2(X_\mathbf{h})\cos(4\pi\mathbf{h}\cdot\mathbf{r}-2\varphi_{p\mathbf{h}})\\ &\quad+\frac{4}{V^2}\sum_{\mathbf{h}\neq\mathbf{k}>0}|F_\mathbf{h}F_\mathbf{k}|m_\mathbf{h}m_\mathbf{k}\cos(2\pi\mathbf{h}\cdot\mathbf{r}-\varphi_{p\mathbf{h}})\\ &\quad\times\cos(2\pi\mathbf{k}\mathbf{r}-\varphi_{p\mathbf{k}}).\end{aligned}\tag{8}$$

Since the last term in equation (8) is equal to

$$\rho^2{}_{\rm obs}(\mathbf{r})-\frac{4}{V^2}\sum_{\mathbf{h}>0}m_\mathbf{h}^2|F_\mathbf{h}|^2\cos^2(2\pi\mathbf{h}\cdot\mathbf{r}-\varphi_{p\mathbf{h}})$$

we obtain

$$\begin{aligned}\langle\rho^2(\mathbf{r})\rangle &= \frac{2}{V^2}\sum_{\mathbf{h}>0}(1-m_\mathbf{h}^2)|F_\mathbf{h}|^2-\frac{2}{V^2}\sum_{\mathbf{h}>0}|F_\mathbf{h}|^2[m_\mathbf{h}^2-D_2(X_\mathbf{h})]\\ &\quad\times\cos(4\pi\mathbf{h}\cdot\mathbf{r}-2\varphi_{p\mathbf{h}})+\rho^2_{\rm obs}(\mathbf{r})\end{aligned}$$

and

$$\begin{aligned}{\rm var}_\rho(\mathbf{r}) &= \langle[(\rho(\mathbf{r})]^2\rangle-[\langle\rho(\mathbf{r})\rangle]^2\\ &= \frac{2}{V^2}\sum_{\mathbf{h}>0}(1-m_\mathbf{h}^2)|F_\mathbf{h}|^2\\ &\quad-\frac{2}{V^2}\sum_{\mathbf{h}>0}|F_\mathbf{h}|^2[m_\mathbf{h}^2-D_2(X_\mathbf{h})]\cos(4\pi\mathbf{h}\cdot\mathbf{r}-2\varphi_{p\mathbf{h}})\end{aligned}\tag{9}$$

or also

$$\begin{aligned}{\rm var}_\rho(\mathbf{r}) &= \frac{2}{V^2}\sum_{\mathbf{h}>0}[1-D_2(X_\mathbf{h})]|F_\mathbf{h}|^2\\ &\quad-\frac{4}{V^2}\sum_{\mathbf{h}>0}|F_\mathbf{h}|^2[m_\mathbf{h}^2-D_2(X_\mathbf{h})]\cos^2(2\pi\mathbf{h}\cdot\mathbf{r}-\varphi_{p\mathbf{h}}).\end{aligned}\tag{10}$$

Equations (9) and (10) are the formulas we were looking for. The corresponding expressions for ${\rm var}_{\rho N}(\mathbf{r})$ are obtained from equations (9) and (10) just by replacing $|F_\mathbf{h}|$ by $R_\mathbf{h}$.

4. The properties of the variance in *P*1

According to equations (9) and (10):

(1) The variance in a point $\mathbf{r}$ is the difference of two contributions: the first (say the *constant term*) does not vary with $\mathbf{r}$, the second (say the *variable term*) depends on $\mathbf{r}$. Since $\cos(4\pi\mathbf{h}\cdot\mathbf{r}-2\varphi_{p\mathbf{h}})\leq 1$ and (see Fig. 1) $1-m_\mathbf{h}^2\geq m_\mathbf{h}^2-D_2(X_\mathbf{h})$, the variance is expected to be non-negative in any point of the unit cell. We will consider the first term of equation (9), rather than the first term of equation (10), as the constant component of the variance. Indeed, if we consider the phases to be statistically independent of each other, the average value of the variable term in equation (9) is zero, while the variable term in equation (10) is never negative because it contains a constant positive component [*i.e.* $\cos^2x=(1+\cos 2x)/2$].

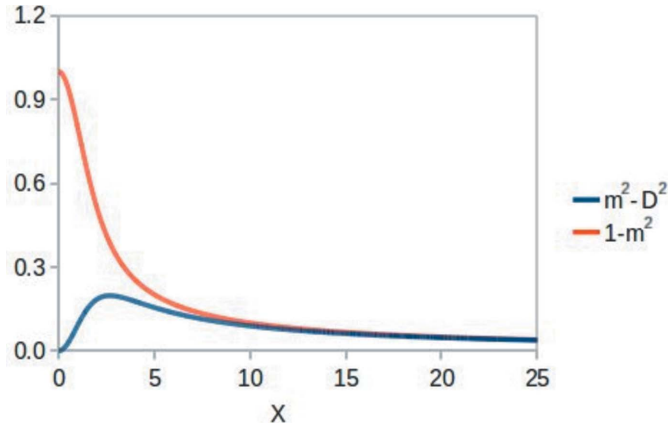

Figure 1
$m_\mathbf{h}^2-D_2(X_\mathbf{h})$ *versus* X, for a suitable interval of X.

(2) $m_\mathbf{h}^2-D_2(X_\mathbf{h})$ is positive for any value of X (see Fig. 1), but for $X=0$ and $X=\infty$, it vanishes. Accordingly, the *variable term* vanishes (that is, the variance is constant for any $\mathbf{r}$) when the model is uncorrelated or when it coincides with the target structure. The reason why, in these conditions, the variance is a constant is easily understandable. If CORR = 0 no phase information is available, and therefore there is no reason that the variance in one point of the cell is different from the variance in another point (*i.e.* the variance is constant and different from zero). If CORR = 1 the phases are distributed according to Dirac delta functions and assume their correct values; the map $\rho(\mathbf{r})$ is then perfectly defined and the variance vanishes in any point of the map.

(3) Large contributions to the *variable term* may arise from reflections with large observed and small calculated amplitudes {for them $|F_\mathbf{h}|^2[m_\mathbf{h}^2-D_2(X_\mathbf{h})]$ is expected to be larger, see Fig. 1}; and, *vice versa*, the contribution is expected to be quite small from reflections for which the observed amplitudes are very small [they do not contribute significantly to $\rho(\mathbf{r})$; see also the last observation in this section].

(4) The three-dimensional periodicity of the variance is half that of the electron density. Indeed it assumes the same value in $\mathbf{r}$ and in $\mathbf{r}+\mathbf{u}$, where $\mathbf{u}=u\mathbf{a}+v\mathbf{b}+w\mathbf{c}$ and u, v, w may be 0 or $\frac{1}{2}$.

(5) As is well known, the $\rho_{\rm obs}(\mathbf{r})$ maxima are located where $\sum_{\mathbf{h}>0}m_\mathbf{h}|F_\mathbf{h}|\cos(2\pi\mathbf{h}\cdot\mathbf{r}-\varphi_{p\mathbf{h}})$ is positive and maximum (*e.g.* at or near to the atomic positions of the model); the minima of the variance are located where $\sum_{\mathbf{h}>0}|F_\mathbf{h}|^2[m_\mathbf{h}^2-D_2(X_\mathbf{h})]\cos^2(2\pi\mathbf{h}\cdot\mathbf{r}-\varphi_{p\mathbf{h}})$ is positive and maximum. Accordingly, the minima of the variance are expected to be close to the points where $\rho_{\rm obs}(\mathbf{r})$ attains its maxima and its minima. Of course, truncation effects due to the limited experimental resolution contribute to displace minima and maxima from the expected positions.

It may be useful to introduce a supplementary point of view. In two recent papers by Burla *et al.* (2006) and Caliandro *et al.* (2007) the main properties of the Fourier synthesis

$$\mathrm{FF} = V^{-1} \sum_{\mathbf{h}>0} |F_{\mathbf{h}}|^2 \cos(2\pi\mathbf{h}\cdot\mathbf{r} - 2\varphi_{\mathbf{h}}) \qquad (11)$$

are described. The authors applied FF to acentric space groups to check for the presence of a pseudocentric phase distribution during Patterson deconvolution phasing procedures. A strong maximum should indicate the presence of a pseudo-inversion centre. The synthesis [equation (11)] attains maxima at the points $\mathbf{r}_i + \mathbf{r}_j$; accordingly the distribution $V^{-1}\sum_{\mathbf{h}>0}|F_{\mathbf{h}}|^2\cos(4\pi\mathbf{h}\cdot\mathbf{r} - 2\varphi_{\mathbf{h}})$ is expected to have maxima at $(\mathbf{r}_i + \mathbf{r}_j)/2$ (there the variance is expected to show minima). The variable term of the variance in equation (9) does not coincide with the synthesis [equation (11)] because it is a weighted observed Fourier synthesis, with a weight that is not proportional to the $2\varphi_{\mathbf{h}}$ reliability. However, it may be expected that the variable term vanishes far away from the atomic positions.

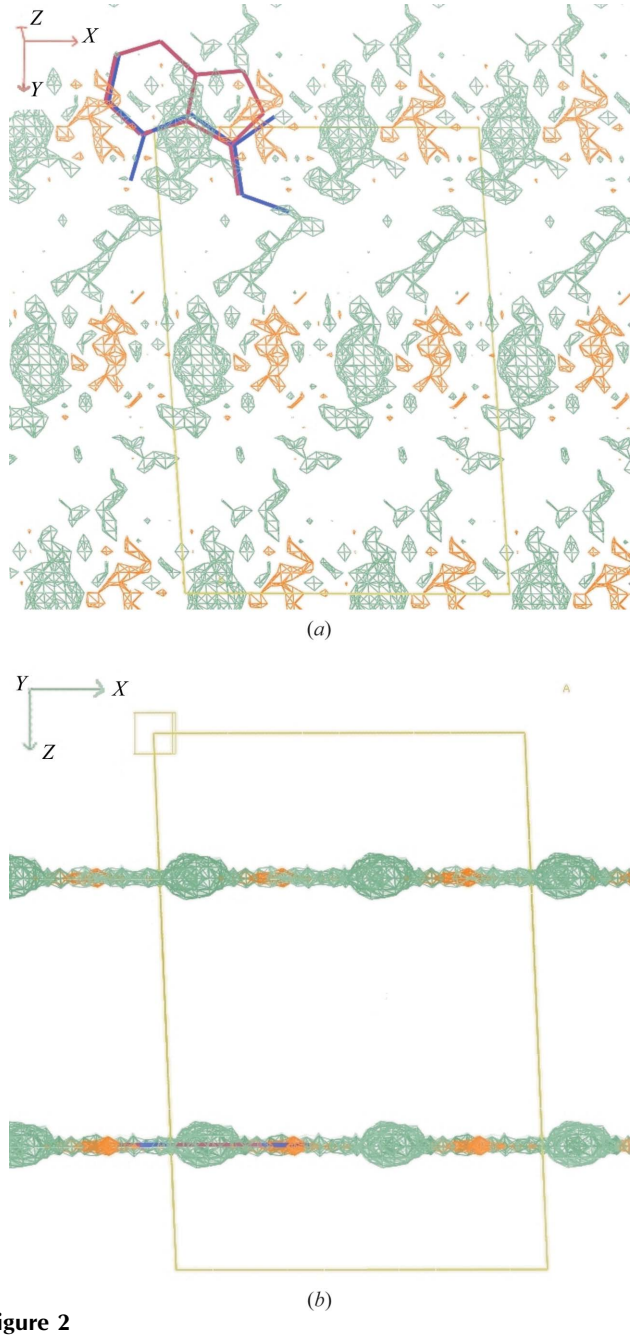

Figure 2
Target (simulated) crystal structure in *P*1: the planar ten-atom molecule (in red in Fig. 2*a*) is on the plane (**a**, **b**). A model (in blue) was generated, for which $\sigma_A = 0.7$, by deleting some of the target atoms. (*a*) and (*b*) show the projection of the *variable term* on the planes (**a**, **b**) and (**a**, **c**), respectively.

To check the above conclusions we simulated a crystal structure in *P*1 characterized by a very large unit cell: a ten-atom planar molecule was located on the plane (**a**, **b**) and a model structure was generated by deleting and moving some of the atoms of the target molecule. In Figs. 2(*a*) and 2(*b*) we show the projection of the variable term on the planes (**a**, **b**) and (**a**, **c**), respectively. The distribution is rather flat (much flatter if the full variance is taken into consideration): minima and maxima are concentrated close to the plane (**a**, **b**) [and, owing to property (4) above, also close to the parallel plane at $c = 1/2$]; it is quite flat in all the other points of the unit cell.

(6) In equation (9) each reflection adds: (i) a positive or negative contribution to the variable term according to whether $\cos(4\pi\mathbf{h}\cdot\mathbf{r} - 2\varphi_{p\mathbf{h}})$ is negative or positive; (ii) an always positive contribution to the constant term, larger than the contribution described in (i) [see Fig. 1 for the difference between $(1 - m_{\mathbf{h}}^2)$ and $m_{\mathbf{h}}^2 - D_2(X_{\mathbf{h}})$]. Accordingly, the value of the constant term is expected to be remarkably larger than the values of the variable term for any **r**.

To verify the effects of the correlation between model and target structure, for the same simulated target structure described in point (5) we created five models with different correlations with the target (the correlation may be estimated by the corresponding $\langle\sigma_A\rangle$ values, where $\langle\sigma_A\rangle$ is the average of the σ_A values calculated per resolution shell). For each of these models we computed the value of

$$\mathrm{oscv} = \left\{\max[\mathrm{var}_\rho(\mathbf{r})] - \min[\mathrm{var}_\rho(\mathbf{r})]\right\}/\mathrm{const}$$

when **r** varies over all the points of the variance map. Oscv provides, for a given variance map, the maximum oscillation of the variance as a percentage of the *constant term* (const in the formula). The values of oscv are plotted in Fig. 3 (blue squares) *versus* the parameter $\langle\sigma_A\rangle$. It may be observed: (i) oscv is in the range 0.14–0.30 for the tested $\langle\sigma_A\rangle$ values; (ii) in accordance with point (i), the variance does not significantly change with the point **r**; (iii) in §5 we will consider $\rho_{\mathrm{obs}}(\mathbf{r})/\sigma_\rho$ as the signal/noise ratio, where $\sigma_\rho = (\mathrm{var}_\rho)^{1/2}$. It is therefore relevant to show (see Fig. 3) the trend of

$$\mathrm{osc}\sigma = \left\{\max[\sigma_\rho(\mathbf{r})] - \min[\sigma_\rho(\mathbf{r})]\right\}/(\mathrm{const})^{1/2}$$

for different values of CORR. It varies in the interval 0.07–0.15. Since $\rho_{\mathrm{obs}}(\mathbf{r})$ varies very strongly with **r**, the value of $\rho_{\mathrm{obs}}(\mathbf{r})/(\sigma_\rho)^{1/2}$ depends mainly on the variation of the observed electron-density distribution.

In accordance with points (i)–(iii) and in order to simplify our study of the variance properties, we will consider the

variance approximately constant for all the points of the unit cell; we do not exclude the possibility, however, that, at a deeper analysis, the variable term may have some role in the phasing procedures in *P*1. From now on

$$\mathrm{var}_\rho(\mathbf{r}) = \mathrm{var}_\rho = \frac{2}{V^2}\sum_{\mathbf{h}>0}(1 - m_{\mathbf{h}}^2)|F_{\mathbf{h}}|^2 \qquad (12a)$$

and

$$\sigma_\rho(\mathbf{r}) = \sigma_\rho = (\mathrm{var}_\rho)^{1/2} \qquad (12b)$$

will represent the *variance of the map* and its *standard deviation*. The above results may be rather unexpected, but are justified by the following observation: for a given CORR value the variance in an atomic position cannot be very different from the variance calculated in a point far from it. Indeed, a small variance in the atomic positions implies that the zero-density points are well estimated. *Vice versa*, a large variance in the atomic positions implies also that the background points are badly estimated.

σ_ρ should not be confused with the standard deviation of the pixel intensity distribution of an electron-density map (let us denote it by σ_d). σ_d is widely used in protein crystallography: very often only those pixels of a map having a density larger than $n\sigma_d$, where n is a suitable rational number, are selected for further calculations. σ_ρ and σ_d have a quite different meaning and therefore a quite different behaviour. To give a numerical idea of the relationship between the two quantities, we plot in Fig. 3 σ_ρ and σ_d *versus* $\langle\sigma_A\rangle$ for the same six models for which we calculated the variance. It is easily seen that σ_ρ and σ_d are anticorrelated: the first diminishes and the second increases when CORR improves.

Let us consider σ_ρ and σ_d trends *versus* data resolution. According to equations (12*a*) and (12*b*) the value of var_ρ, and therefore of σ_ρ, for a given model, increases in the case of better data resolution [in this case the summation on the right-hand side of equation (12*a*) involves a larger number of terms]. Also σ_d increases when the resolution improves (then positive peaks are stronger). In Fig. 4, for the protein PDB (Protein Data Bank) refcode 1bxo with RES = 0.95, and for two model structures with a mean phase error with respect to the target (say MPE) equal to 45 and 66°, respectively, we show the values of σ_ρ and of σ_d when the data are cut at different resolutions. We observe: (i) σ_ρ and σ_d curves do not coincide but show a similar trend with the resolution; (ii) $\sigma_d \gg \sigma_\rho$ for the better correlated model, but $\sigma_d < \sigma_\rho$ for the poor model. That agrees well with Fig. 3: indeed σ_A = 0.16 for the poor model, σ_A = 0.43 for the better correlated model.

Both σ_ρ and σ_d decrease when the average thermal factor increases (*e.g.* because the moduli $|F_{\mathbf{h}}|^2$ decrease more rapidly with increasing values of $\sin\theta/\lambda$), and both depend on the density of the scattering power of the target structure (σ_ρ and σ_d will be different for two structures with identical atomic positions but with different scattering power).

If *E* maps are used, σ_ρ and σ_d are expected to have a sharper trend. Indeed, in this case we deal with non-band-limited distributions: then $\langle R^2\rangle = 1$ no matter the resolution shell. In this situation σ_ρ and σ_d are expected to increase very rapidly with RES, much more than for *F* maps.

The consequences of the above conclusions cannot be fully estimated if one does not consider how the electron density itself varies with the parameters considered above. We will discuss this point in §6.

A last point deserves to be examined. In a recent paper Caliandro *et al.* (2008) assumed, as in this work, that a model structure is available and that each phase $\varphi_{\mathbf{h}}$ is distributed around $\varphi_{p\mathbf{h}}$ according to equation (3). They focused their attention on the difference electron density, and derived for the corresponding Fourier coefficients the variance expression

$$\sigma_{q_{\mathbf{h}}} = (1 - m^2)|F_{\mathbf{h}}|^2.$$

The result was obtained by assuming the model parameters to be constants of the mathematical approach; as a consequence, the above equation may also be applied not only to the difference electron density but also to the electron density

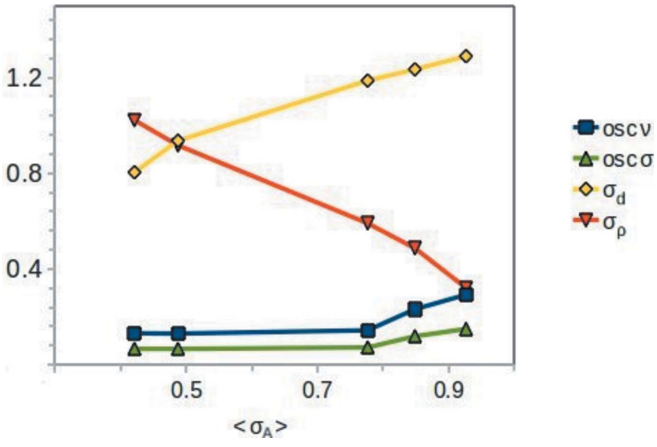

Figure 3
Oscv (blue line), oscσ (green line), σ_ρ (red line) and σ_d (yellow lines) are plotted *versus* $\langle\sigma_A\rangle$. The five blue and yellow squares, and the red and yellow triangles correspond to the five models of the simulated target structure described in the text.

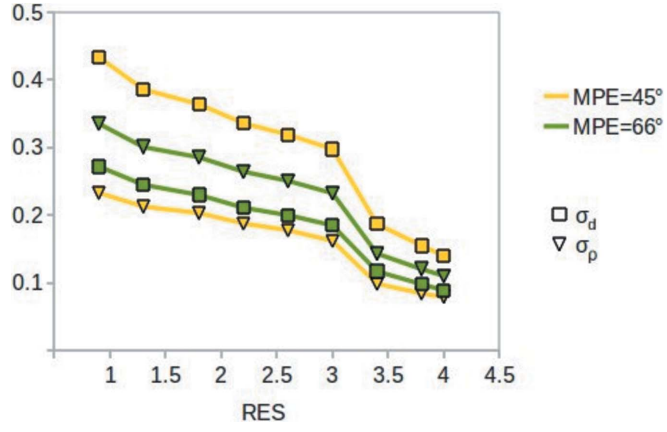

Figure 4
Protein 1bxo: σ_ρ (triangles) and σ_d (squares) *versus* RES for two model structures, having MPE = 45° (yellow) and 66° (green), respectively.

itself (see also §5). Accordingly, var_ρ is nothing else but the sum of the variances of the single reflections, considered statistically independent, divided by the squared unit-cell volume:

$$\mathrm{var}_\rho(\mathbf{r}) = \frac{1}{V^2}\sum_{\mathbf{h}} \sigma^2_{q\mathbf{h}}.$$

If the distribution of the phases is considered independent of the distribution of measurement errors (that is a reasonable assumption because errors on measurements depend on the experiment, while the phase distribution depends on the model), we can combine equations (2) and (12*a*) into

$$\mathrm{var}_\rho(\mathbf{r}) = \frac{2}{V^2}\sum_{\mathbf{h}>0} [2\sigma^2(|F_\mathbf{h}|)\cos^2(2\pi\mathbf{h}\cdot\mathbf{r} - \varphi_\mathbf{h}) + (1 - m^2_\mathbf{h})|F_\mathbf{h}|^2], \tag{13a}$$

providing the variance map for any electron density, no matter the degree of correlation between model and target structures.

If the correlation between model and target structures is not very high, the contribution to the variance arising from measurement errors is negligible; indeed it depends on $\sigma^2(|F_\mathbf{h}|)$, which is usually quite a small percentage of the $|F_\mathbf{h}|^2$ moduli. The contribution arising from weak reflections, for which measurement errors are comparable with diffraction amplitudes, may be neglected with respect to that provided by strong reflections.

Vice versa, at the end of a satisfactory structure refinement, $m^2_\mathbf{h}$ is close to unity for nearly all the reflections, the variance is mainly determined by measurement errors and varies from point to point in the map. It may be worthwhile noticing that some inadequacy of the refined structural model may cause uncertainty on some phases, in particular on the weak reflection phases, which may be characterized by non-unitary $m^2_\mathbf{h}$ values. In this case the contribution to the variance arising from the phase distribution is no longer negligible and may substantially contribute to the total map variance. It may also occur that the variable term, described in §4, may play some role in a better definition of the variance; specific experimental tests should be useful to confirm the conjecture.

If the electron-density map is calculated by normalized structure factors, then

$$\begin{aligned}\mathrm{var}_{\rho N}(\mathbf{r}) &= \mathrm{var}_{\rho N} \\ &= \frac{2}{V^2}\sum_{\mathbf{h}>0}\Big[\sum_{\mathbf{h}>0}\sigma^2(|E_\mathbf{h}|)\cos^2(2\pi\mathbf{h}\cdot\mathbf{r} - \varphi_\mathbf{h}) \\ &\quad + (1 - m^2_\mathbf{h})|E_\mathbf{h}|^2\Big].\end{aligned} \tag{13b}$$

5. The estimate of the expected maps and of the variances for some Fourier syntheses

We will consider three types of difference Fourier synthesis, under the assumption that each phase $\varphi_\mathbf{h}$ is distributed on the trigonometric circle according to equation (3).

5.1. Case 1, the ideal difference Fourier synthesis

Let

$$\rho_q(\mathbf{r}) = \rho(\mathbf{r}) - \rho_p(\mathbf{r}) = \frac{2}{V}\sum_{\mathbf{h}>0}|F_{q\mathbf{h}}|\cos(2\pi\mathbf{h}\cdot\mathbf{r} - \varphi_{q\mathbf{h}}). \tag{14}$$

The corresponding map is calculated *via* the coefficients

$$F_{q\mathbf{h}} = |F_{q\mathbf{h}}|\exp(i\varphi_{q\mathbf{h}}) = |F|\exp(i\varphi_\mathbf{h}) - |F_p|\exp(i\varphi_{p\mathbf{h}}). \tag{15}$$

Since the phases $\varphi_\mathbf{h}$ are supposed unknown, we can only estimate the expected value of $\rho_q(\mathbf{r})$:

$$\begin{aligned}\langle\rho_q(\mathbf{r})\rangle &= \langle\rho(\mathbf{r})\rangle - \rho_p(\mathbf{r}) = \rho_{\mathrm{obs}}(\mathbf{r}) - \rho_p(\mathbf{r}) \\ &= \frac{2}{V}\sum_{\mathbf{h}>0}(m_\mathbf{h}|F_\mathbf{h}| - |F_{p\mathbf{h}}|)\cos(2\pi\mathbf{h}\cdot\mathbf{r} - \varphi_{q\mathbf{h}}).\end{aligned} \tag{16}$$

Equation (16) agrees with Main (1979), Burla, Caliandro *et al.* (2010) and Burla, Giacovazzo & Polidori (2010). Since $\rho_p(\mathbf{r})$ is the prior information, it is constant with respect to the chosen set of variables; accordingly the variance of $\rho_q(\mathbf{r})$ (say $\mathrm{var}\rho_q$) will satisfy the condition

$$\mathrm{var}_{\rho q} = \mathrm{var}_\rho. \tag{17}$$

5.2. Case 2, the weighted ideal difference electron density

Let

$$\rho_{\mathrm{w}q} = \rho - \langle\sigma_A\rangle\rho_p = \frac{2}{V}\sum_{\mathbf{h}>0}|F_{\mathrm{w}q\mathbf{h}}|\cos(2\pi\mathbf{h}\cdot\mathbf{r} - \varphi_{\mathrm{w}q\mathbf{h}}), \tag{18}$$

where

$$F_{q\mathrm{w}\mathbf{h}} = |F_{\mathrm{w}q\mathbf{h}}|\exp(i\varphi_{\mathrm{w}q\mathbf{h}}) = |F|\exp(i\varphi_\mathbf{h}) - \langle\sigma_A\rangle|F_p|\exp(i\varphi_{p\mathbf{h}}). \tag{19}$$

The parameter σ_A in equation (18) may be defined as $\langle\sigma_A\rangle = \langle\sigma_A(s)\rangle$, where $\sigma_A(s)$ is the σ_A value calculated for the resolution corresponding to s.

The expected value of $\rho_{\mathrm{w}q}(\mathbf{r})$ may be calculated as follows:

$$\begin{aligned}\langle\rho_{\mathrm{w}q}(\mathbf{r})\rangle &= \langle\rho(\mathbf{r})\rangle - \langle\sigma_A\rangle\rho_p(\mathbf{r}) = \rho_{\mathrm{obs}}(\mathbf{r}) - \langle\sigma_A\rangle\rho_p(\mathbf{r}) \\ &= \frac{2}{V}\sum_{\mathbf{h}>0}(m_\mathbf{h}|F_\mathbf{h}| - \langle\sigma_A\rangle|F_{p\mathbf{h}}|)\cos(2\pi\mathbf{h}\cdot\mathbf{r} - \varphi_{p\mathbf{h}}).\end{aligned} \tag{20}$$

Since $\langle\sigma_A\rangle\rho_p$ is a constant with respect to the chosen set of variables, the variance of $\rho_{\mathrm{w}q}$ is given by

$$\mathrm{var}_{\rho\mathrm{w}q} = \mathrm{var}_{\rho q} = \mathrm{var}_\rho. \tag{21}$$

5.3. Case 3, the hybrid ideal difference electron density

Let τ and ω be any pair of real numbers, and

$$\rho_Q(\mathbf{r}) = \tau\rho(\mathbf{r}) - \omega\rho_p(\mathbf{r}) = \frac{2}{V}\sum_{\mathbf{h}>0}|F_Q|\cos(2\pi\mathbf{h}\cdot\mathbf{r} - \varphi_Q). \tag{22}$$

Its Fourier coefficients are

$$F_Q = \tau|F_{\mathbf{h}}|\exp(i\varphi_{\mathbf{h}}) - \omega|F_{p\mathbf{h}}|\exp(i\varphi_{p\mathbf{h}})$$

and its mean value is

$$\langle\rho_Q(\mathbf{r})\rangle = \frac{2}{V}\sum_{\mathbf{h}>0}(\tau m|F_{\mathbf{h}}| - \omega|F_{p\mathbf{h}}|)\cos(2\pi\mathbf{h}\cdot\mathbf{r} - \varphi_{p\mathbf{h}}). \quad (23)$$

Accordingly

$$\mathrm{var}\rho_Q(\mathbf{r}) = \tau^2\mathrm{var}\rho_q(\mathbf{r}) = \tau^2\mathrm{var}\rho(\mathbf{r}). \quad (24)$$

For all the three cases described above, the variance will show the same trend (*versus* the resolution or *versus* CORR) described in §4. Of particular interest is the use of the variance for assessing the meaningfulness of the difference electron density when CORR is close to unity: after the structure refinement, owing to some residual inadequacy of the model, the variance may be determined by the combined contribution arising from the uncertainty on some phases (usually those associated with weak amplitudes) and from measurement errors. In this case the *variable term* in the variance expression may not be negligible. It is worthwhile noticing that we assumed an ideal scaling in our treatment of the difference electron density (and in general for all the hybrid syntheses). However, as observed by Rees (1976, 1978), the meaningfulness of the variance also depends on the correct scaling between $\rho(\mathbf{r})$ and $\rho_p(\mathbf{r})$, a condition quite critical for multipolar refinement in electron-density studies.

6. The signal/noise ratio in electron-density maps

In §3 we showed that, if the phases are assumed to be distributed on the trigonometric circle according to equation (3), the variance of the electron density $\rho(\mathbf{r})$ in $P1$ does not vary significantly with $\mathbf{r}$; in simple terms, it is nearly constant, no matter if $\mathbf{r}$ is on, close to, or far from the atomic positions, and no matter the value of the electron density in that point. We observed in addition that the value of var_ρ, for a given model, increases when the resolution improves, decreases when the average thermal factor increases and depends on the density of the scattering power of the target structure. The above statements hold also for the various types of difference Fourier synthesis, and are rather surprising if one does not consider the corresponding changes of $\rho_{\mathrm{obs}}(\mathbf{r})$, $\langle\rho_q(\mathbf{r})\rangle$, $\langle\rho_{\mathrm{w}q}(\mathbf{r})\rangle$ and $\langle\rho_Q(\mathbf{r})\rangle$. We will show that such properties are the basis of most of the modern successful phasing procedures.

Let us first consider the $\rho(\mathbf{r})$ map. It is accessible only at the end of the phasing procedure: during the phasing process $\rho_{\mathrm{obs}}(\mathbf{r})$ is its best approximation, and may be considered the available signal. Consequently, more than the variance in itself, we have to consider the quantity

$$S(\mathbf{r})/N = \rho_{\mathrm{obs}}(\mathbf{r})/(\mathrm{var}_\rho)^{1/2}, \quad (25)$$

which may be considered the 'signal-to-noise ratio'. For example, when data resolution improves, both $\rho_{\mathrm{obs}}(\mathbf{r})$ and var_ρ increase: the ratio [equation (25)], calculated in the peak sites, can establish if atoms are located with less or greater accuracy. If normalized structure factors are used for calculating the electron-density maps, equation (25) changes to

$$S(\mathbf{r})/N = \rho_{\mathrm{obs}N}(\mathbf{r})/(\mathrm{var}_{\rho N})^{1/2}.$$

Let us now suppose that $\rho_{\mathrm{obs}}(\mathbf{r})$ has been calculated and we want to apply EDM techniques for improving the model. Since var_ρ is constant, in the absence of any additional prior information (which, however, is often available in protein crystallography, *e.g.* knowledge of the envelope), the only way of selecting the pixels with the largest $S(\mathbf{r})/N$ value is the use of a threshold TRH on the $\rho_{\mathrm{obs}}(\mathbf{r})$ densities. Then, automatically, the threshold selects the pixels for which $S(\mathbf{r})/N$ is larger.

An inverse Fourier synthesis based on the selected pixels may lead to phase values better than those used for the calculation of $\rho_{\mathrm{obs}}(\mathbf{r})$ (it is a sort of clean-up technique). This criterion is used in some EDM procedures (Shiono & Woolfson, 1992; Refaat & Woolfson, 1993; Giacovazzo & Siliqi, 1997).

If the main interest is to drastically modify a model without destroying it, a good way is reversing the sign of the density in some region of the map (no matter if in the positive or in the negative region). If this technique is used for *ab initio* phasing, the region to reverse cannot be part of the solution, otherwise convergence would never be reached. *Charge flipping* (Oszlányi & Sütő, 2004, 2005, 2007; Palatinus & Chapuis, 2007) uses exactly this technique: it cyclically reverses the sign of a small sheet of an electron-density map with density close to zero. When a good model is obtained, reversing the sign of $S(\mathbf{r}) >$ TRH in this region provides a negligible perturbation of the model which cannot destroy it.

The technique is also used in non-*ab initio* phasing, when it is fruitful to perturb the model in order to obtain, *via* EDM techniques, a better convergence to the correct phases (Abrahams & Leslie, 1996).

As stated before, the number of pixels with positive density for which $S(\mathbf{r})/N >$ TRH increases with CORR, provided TRH is sufficiently large. As a consequence, those EDM techniques that use, for the Fourier map inversion, a fixed percentage of pixels [for example, 2–4%, those with the largest positive density – this is the case of Giacovazzo & Siliqi (1997) and Burla, Giacovazzo & Polidori (2010) in the VLD algorithm] practically use a different $S(\mathbf{r})/N$ threshold in each inversion cycle (on supposing that CORR changes from cycle to cycle).

A different strategy, fixing the same TRH value for all the EDM cycles, implies the variation of the percentage of the pixels (say PERC) used for the Fourier inversion. According to this last criterion, if CORR improves, PERC automatically increases. The two strategies may produce quite different results when used in automatic EDM procedures. In Fig. 5 we show the trend of the average phase error (MPE) for a small-molecule structure (SCHWARZ, $C_{46}H_{70}O_{27}$; Sheldrick, 1982) and for a medium-sized molecule (TVAL, $C_{54}H_{90}N_6O_{18}$, $Z = 2$; Loll *et al.*, 1997) both crystallizing in $P1$. Phase refinement starts from 72° for SCHWARZ and from 76° for TVAL. In one phase-refinement strategy PERC is maintained constant

(equal to 3%; Giacovazzo & Siliqi, 1997): after 100 EDM cycles MPE drops to 45 and 39° for SCHWARZ and TVAL, respectively. It may be noted that, assuming PERC = 3% at the beginning of the EDM refinement, this corresponds to fixing TRH to 1.57 and 1.77 for SCHWARZ and TVAL, respectively. At cycle 100 PERC = 3% corresponds to TRH = 4.86 and 5.58, respectively, for SCHWARZ and TVAL.

If, during the EDM cycles, the threshold TRH = $S(\mathbf{r})/N$ for SCHWARZ and TVAL is constantly fixed to 1.57 and 1.77, respectively, then MPE drops to 21 and 24° in 100 EDM cycles. The PERC values corresponding to TRH = 1.57 and 1.77 are 3% for both SCHWARZ and TVAL at EDM cycle 1, 14% and 13% at cycle 100.

The above results show that the two strategies may provide quite different results. It cannot be claimed, however, that one is better than the other: many extended tests are necessary, taking into account data resolution, structure size, average thermal factor *etc*. Nevertheless, the results described above indicate that an investigation taking into account the ratio $S(\mathbf{r})/N$ may be rewarding.

7. The signal/noise ratio in difference and hybrid Fourier maps

We will analyse the values of $S(\mathbf{r})/N$ in the difference electron densities considered in §5, and we will compare them with the corresponding ratios of the $\rho(\mathbf{r})$ map. The comparison will confirm the most relevant properties of such maps.

7.1. Case 1, ideal difference Fourier synthesis

Here

$$S(\mathbf{r})/N = [\rho_{\rm obs}(\mathbf{r}) - \rho_p(\mathbf{r})]/(\mathrm{var}_\rho)^{1/2}. \quad (26)$$

We observe:

(*a*) When CORR $\sim$ 0, according to equations (12*a*) and (12*b*), var_ρ attains its maximum; then equation (26) coincides with

$$S(\mathbf{r})/N = -\rho_p(\mathbf{r})/(\mathrm{var}_\rho)^{1/2}. \quad (27)$$

If the random model has the same global scattering power of the target, the value of $S(\mathbf{r})/N$ provided by $-\rho_p(\mathbf{r})$ (calculated in correspondence with the peaks in the map) is large and comparable with that obtained by an observed electron density highly correlated with the target. The meaning of the signal is however different: in the case of equation (27) the negative peaks of the map suggest eliminating the model, in the observed map case the peak positivity confirms the model. The signal provided by equation (27) diminishes with its scattering power [*i.e.* it is more informative to generate a large random scattering model than a small one; see Burla, Giacovazzo & Polidori (2010)]. It may be concluded, according to Burla, Caliandro *et al.* (2010), that a model, even if random, may provide, through the difference Fourier synthesis [equation (16)], reliable information on $\rho_q(\mathbf{r})$ because the signal-to-noise ratio is high. The reader is referred to Table 2 of that paper to check this surprising result: in the table $\langle\Delta\varphi_q\rangle$, the average phase error on the phase φ_q, is shown for some random models.

(*b*) When CORR increases the amplitude of the positive peaks in $\rho_{\rm obs}(\mathbf{r}) - \rho_p(\mathbf{r})$ increases while the denominator of the right-hand side of equation (27) diminishes. Then positive peaks start to be part of a new model, and negative peaks tend to vanish where $\rho_{\rm obs}(\mathbf{r})$ nearly overlaps with $\rho_p(\mathbf{r})$. To check how $S(\mathbf{r})/N$ varies with CORR we calculated its largest positive and negative values for the five examples used in §3. The results are shown in Fig. 6. As expected, the largest absolute values of $S(\mathbf{r})/N$ for loosely correlated models are obtained for the curve $(S/N-)$ (where it reaches the value -19, corresponding to a model atom in a false position). The largest positive value of $S(\mathbf{r})/N$ is obtained for the curve $(S/N+)$ (where it reaches the value of 25, corresponding to a missed atom). Obviously, the largest positive ratios $S(\mathbf{r})/N$ are obtained for observed electron densities, where values close to 65 are observed.

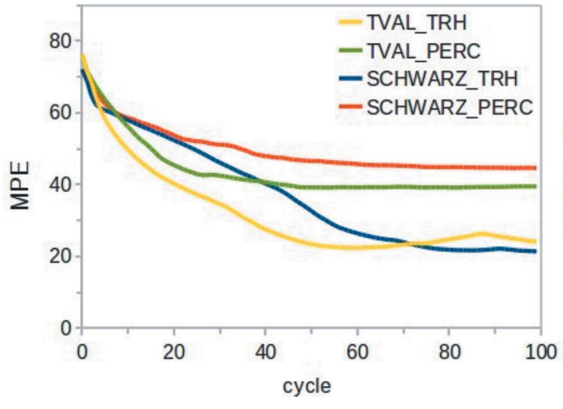

Figure 5
SCHWARZ and TVAL: mean phase error (MPE) *versus* EDM cycles. TRH and PERC indicate the EDM strategies: in the first case the threshold TRH = $S(\mathbf{r})/N$ is maintained fixed, in the second case the percentage of the pixels used in the Fourier inversion is constant.

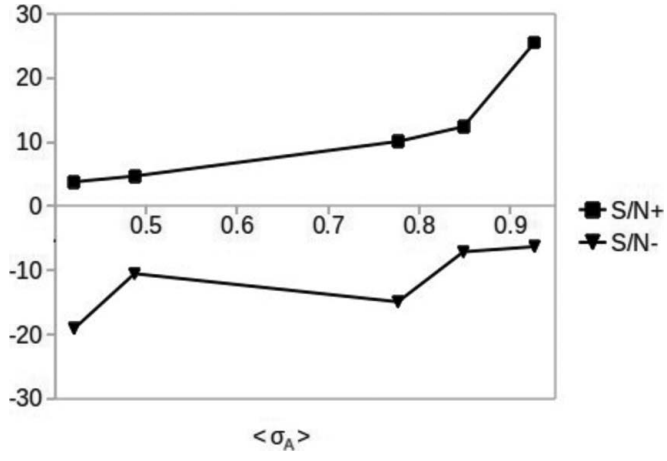

Figure 6
The largest positive $(S/N+)$ and largest negative $(S/N-)$ values of $S(\mathbf{r})/N$ for the five models of the simulated target structure described in §3. On the abscissa are the corresponding $\langle\sigma_A\rangle$ values.

7.2. Case 2, weighted difference electron density

We notice:

(*a*) According to equations (18) and (20) the signal-to-noise ratio is given by

$$S(\mathbf{r})/N = [\rho_{\rm obs}(\mathbf{r}) - \langle\sigma_A\rangle\rho_p(\mathbf{r})]/(\mathrm{var}_\rho)^{1/2}. \quad (28)$$

(*b*) For an uncorrelated model the signal vanishes: no information is provided on the ideal $\rho_q(\mathbf{r})$.

(*c*) For increasing values of CORR, in equation (28) the numerator increases and the denominator decreases. The map becomes more informative.

Both the properties (*b*) and (*c*) are also known features of the difference maps calculated with Read (1986) coefficients $(m_{\mathbf{h}}|F_{\mathbf{h}}| - D|F_{p\mathbf{h}}|)\exp(i\varphi_{p\mathbf{h}})$ or $(m_{\mathbf{h}}|R_{\mathbf{h}}| - \sigma_A|R_{p\mathbf{h}}|)\exp(i\varphi_{p\mathbf{h}})$.

7.3. Case 3, hybrid ideal difference electron density

According to equations (23) and (24)

$$\frac{S(\mathbf{r})}{N} = \frac{\tau\rho_{\rm obs}(\mathbf{r}) - \omega\rho_p(\mathbf{r})}{\tau[\mathrm{var}\rho(\mathbf{r})]^{1/2}}. \quad (29)$$

We will comment on equation (29) according to two parameters, τ/ω and CORR:

(*a*) When CORR ~ 0 var_ρ attains its maximum value and equation (29) coincides with

$$S(\mathbf{r})/N = -\omega\rho_p(\mathbf{r})/\tau(\mathrm{var}_\rho)^{1/2}. \quad (30)$$

The signal (constituted by the negative peaks of the $-\rho_p$ map) is maximized for large scattering power of the random model and diminishes when the ratio τ/ω increases (the variance increases with τ^2); as a consequence the Fourier syntheses with $\tau > \omega$ are expected to be less correlated with the ideal electron density ρ_Q. This is the case of the widely used Fourier synthesis characterized by $\tau = 2$ and $\omega = 1$, which is mostly employed for its capacity of reducing the model bias rather than for immediately providing a better map correlation.

(*b*) The value of $S(\mathbf{r})/N$ increases with increasing values of ω/τ: maps with high values of ω/τ are expected to provide, *via* the negative peaks, high-quality information on φ_Q, particularly for random models.

(*c*) The amplitude of the positive peaks in $\tau\rho_{\rm obs}(\mathbf{r}) - \omega\rho_p(\mathbf{r})$ increases with increasing values of CORR, and the quality of the signal improves proportionally to the value of τ. For large τ values positive peaks may easily become part of a new model. It may be concluded that Fourier syntheses with $\tau > \omega$ may be electively employed for models with sufficiently high correlation with the target, to reduce the model bias and at the same time to improve the correlation. Fourier syntheses with $\tau < \omega$ are more useful when applied to very poor models, for drastically changing them up to when a satisfactory model is achieved. Paradoxically, such types of hybrid Fourier synthesis are less often used in crystallography.

8. Conclusions

A new approach for calculating in *P*1 the variance of electron-density maps is described. Observed, difference and hybrid electron densities are considered under the assumption that the phases are distributed on the trigonometric circle according to von Mises distributions centred on the correct phase values. A general formula for the variance was obtained: it does not remarkably change with **r**, no matter if **r** is located on a peak or on a low-density point. The concept of *map variance* was then introduced, and its dependence on various parameters (*e.g.* correlation between model and target structure, resolution *etc.*) was studied.

The results were used to analyse the quality of the information provided by any type of density map through a criterion of type 'signal to noise'. Such criterion enabled us to correlate the variance properties with the most successful phasing procedures.

For reader usefulness it is anticipated that the concept of *map variance* does not hold for space groups with symmetry higher than *P*1. This property opens new perspectives for the phasing procedures: indeed, according to this result, two points of an electron-density map may have the same density but a different variance, and therefore they may have different signal-to-noise values.

References

Abrahams, J. P. & Leslie, A. G. W. (1996). *Acta Cryst.* D**52**, 30–42.
Booth, A. D. (1946). *Proc. R. Soc. London Ser. A*, **188**, 77–92.
Booth, A. D. (1947). *Proc. R. Soc. London Ser. A*, **190**, 482–489.
Bragg, W. L. & West, J. (1930). *Philos. Mag.* **10**, 823–824.
Burla, M. C., Caliandro, R., Carrozzini, B., Cascarano, G. L., De Caro, L., Giacovazzo, C., Polidori, G. & Siliqi, D. (2006). *J. Appl. Cryst.* **39**, 527–535.
Burla, M. C., Caliandro, R., Giacovazzo, C. & Polidori, G. (2010). *Acta Cryst.* A**66**, 347–361.
Burla, M. C., Giacovazzo, C. & Polidori, G. (2010). *J. Appl. Cryst.* **43**, 825–836.
Caliandro, R., Carrozzini, B., Cascarano, G. L., De Caro, L., Giacovazzo, C. & Siliqi, D. (2007). *J. Appl. Cryst.* **40**, 883–890.
Caliandro, R., Carrozzini, B., Cascarano, G. L., De Caro, L., Giacovazzo, C. & Siliqi, D. (2008). *Acta Cryst.* A**64**, 519–528.
Cochran, W. (1951). *Acta Cryst.* **4**, 408–411.
Coppens, P. & Hamilton, W. C. (1968). *Acta Cryst.* B**24**, 925–929.
Cruickshank, D. W. J. (1949). *Acta Cryst.* **2**, 65–82.
Cruickshank, D. W. J. & Rollett, J. S. (1953). *Acta Cryst.* **6**, 705–707.
Giacovazzo, C. & Siliqi, D. (1997). *Acta Cryst.* A**53**, 789–798.
Loll, P. J., Bevivino, A. E., Korty, B. D. & Axelsen, P. H. (1997). *J. Am. Chem. Soc.* **119**, 1516–1522.
Main, P. (1979). *Acta Cryst.* A**35**, 779–785.
Oszlányi, G. & Sütő, A. (2004). *Acta Cryst.* A**60**, 134–141.
Oszlányi, G. & Sütő, A. (2005). *Acta Cryst.* A**61**, 147–152.
Oszlányi, G. & Sütő, A. (2007). *Acta Cryst.* A**63**, 156–163.
Palatinus, L. & Chapuis, G. (2007). *J. Appl. Cryst.* **40**, 786–790.
Read, R. J. (1986). *Acta Cryst.* A**42**, 140–149.
Rees, B. (1976). *Acta Cryst.* A**32**, 483–488.
Rees, B. (1978). *Acta Cryst.* A**34**, 254–256.
Refaat, L. S. & Woolfson, M. M. (1993). *Acta Cryst.* D**49**, 367–371.
Sheldrick, G. M. (1982). *Testing Structures for Direct Methods*. University of Cambridge, UK.
Shiono, M. & Woolfson, M. M. (1992). *Acta Cryst.* A**48**, 451–456.
Srinivasan, R. & Ramachandran, G. N. (1965). *Acta Cryst.* **19**, 1008–1014.